Gallium arsenide deep-level optical emitter for fibre optics

JANET L. PAN*, JOSEPH E. MCMANIS, THOMAS OSADCHY, LOUISE GROBER, JERRY M. WOODALL AND PETER J. KINDLMANN

Yale University, PO Box 208284, New Haven, Connecticut 06520-8284, USA

*e-mail: janet.pan@yale.edu

Published online: 4 May 2003; doi:10.1038/nmat887

Fibre-optic components fabricated on the same substrate as integrated circuits are important for future high-speed communications. One industry response has been the costly push to develop indium phosphide (InP) electronics. However, for fabrication simplicity, reliability and cost, gallium arsenide (GaAs) remains the established technology for integrated optoelectronics. Unfortunately, the GaAs bandgap wavelength (0.85 μm) is far too short for fibre optics at 1.3–1.5 μm. This has led to work on materials that have a large lattice mismatch on GaAs. Here we demonstrate the first light-emitting diode (LED) that emits at 1.5 μm fibre-optic wavelengths in GaAs using optical transitions from arsenic antisite (As_{Ga}) deep levels. This is an enabling technology for fibre-optic components that are lattice-matched to GaAs integrated circuits. We present experimental results showing significant internal optical power (24 mW) and speed (in terahertz) from GaAs optical emitters using deep-level transitions. Finally, we present theory showing the ultimate limit to the efficiency-bandwidth product of semiconductor deep-level optical emitters.

We have created artificial deep-level energy bands by molecular-beam epitaxy (MBE) of low-temperature-grown GaAs (LTG-GaAs). LTG-GaAs has a number of properties useful for devices. More than 10^{20} cm^{-3} of As_{Ga} can be incorporated[1,2] into LTG-GaAs. This large amount of As_{Ga} results in larger absorption coefficients (and thus larger efficiency-bandwidth products) for deep-level optical transitions—about as large[3,4] as for conventional conduction-to-valence band transitions. Here, we will demonstrate strong optical emission peaks at 1 μm and1.5 μm from LTG-GaAs. LTG-GaAs is transparent from very long infrared wavelengths to 1.8 μm (Fig. 1.) This is significant because it shows that the deep-level energy band has moved the absorption edge to 1.8 μm (conventional GaAs has a bandgap wavelength of 0.85 μm). Finally, LTG-GaAs has short (subpicosecond) carrier lifetimes, and could be used for high-speed applications.

Figure 2a shows the lifetimes for radiative (τ_R) and non-radiative transitions (τ_{NR}) from an upper to a lower state. For the states shown in Fig. 2b for LTG-GaAs, $1/\tau_{C1}$ is the total rate of all transitions between the conduction-band electron and As_{Ga}^{+}; $1/\tau_{NR}$ and $1/\tau_R$ are, respectively, the non-radiative and radiative rates of transitions between the valence-band hole and As_{Ga}. Both the turn-off time and the turn-on time (for example, decay time[5–7] of relaxation oscillations) of optical emitters are determined by the below-threshold total relaxation rate ($1/\tau_R + 1/\tau_{NR}$) of

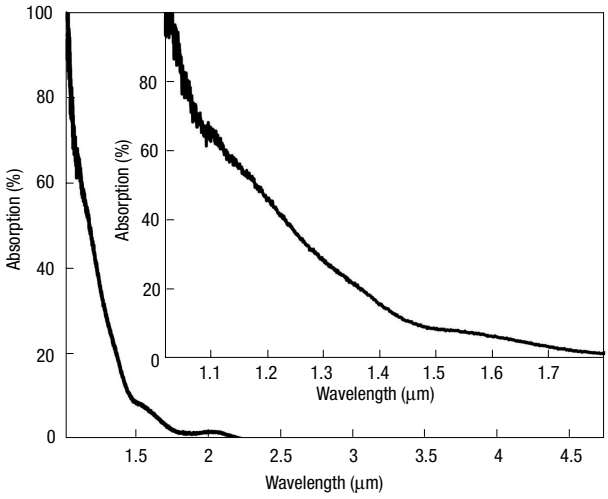

Figure 1 Absorption spectrum measured at room temperature of 1 μm of GaAs grown at 225 °C. The inset shows the measured absorption between 1.0 μm and 1.8 μm.

carriers from the upper state to the lower state of the optical transition. The internal radiative efficiency is $\eta_R = \tau_{NR}/(\tau_R + \tau_{NR})$. Thus, the efficiency-bandwidth product is $\eta_R(1/\tau_R + 1/\tau_{NR}) = 1/\tau_R$, and is determined by the radiative lifetime τ_R. Large efficiency-bandwidth products are thus associated with fast τ_R (strong optical transitions).

Absorption is one measure of the optical transition strength. Figure 1 shows that our experimentally measured absorption for LTG-GaAs is 10^4 cm^{-1} and 1.6×10^3 cm^{-1} at 1.1 μm and 1.55 μm, respectively. Thus, the measured absorption from deep-levels in LTG-GaAs is almost as large as for conventional conduction-to-valence band transitions.

Energy-band theory[3,4] can predict the selection rules and large strength of optical transitions from deep-levels in a wide variety of semiconductors. The deep states can be found by analytically continuing the conduction and valence bands into the bandgap. The general optical properties of deep levels can then be explained in

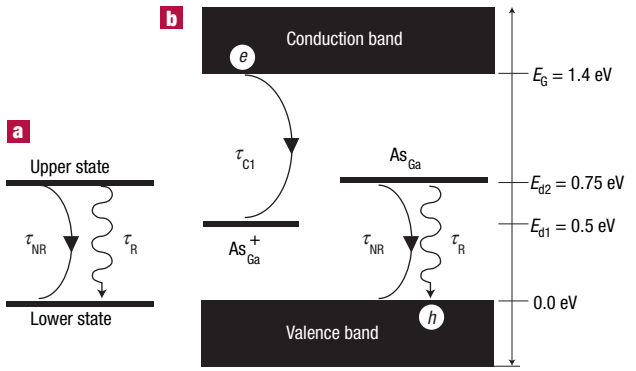

Figure 2 Energy levels and transition rates. a, Radiative lifetimes (τ_R) and non-radiative lifetimes (τ_{NR}) associated with transitions from an upper state to a lower state. **b**, τ_R, τ_{NR} and total transition lifetimes (τ_{C1}) associated with transitions[11] (to As_{Ga}^+ and from As_{Ga}) in low-temperature-grown GaAs; *e* is electron and *h* is hole. E_G, E_{d2} and E_{d1} are, respectively, the energies of the conduction-band edge, of As_{Ga}^+, and of As_{Ga}, relative to the valance-band edge.

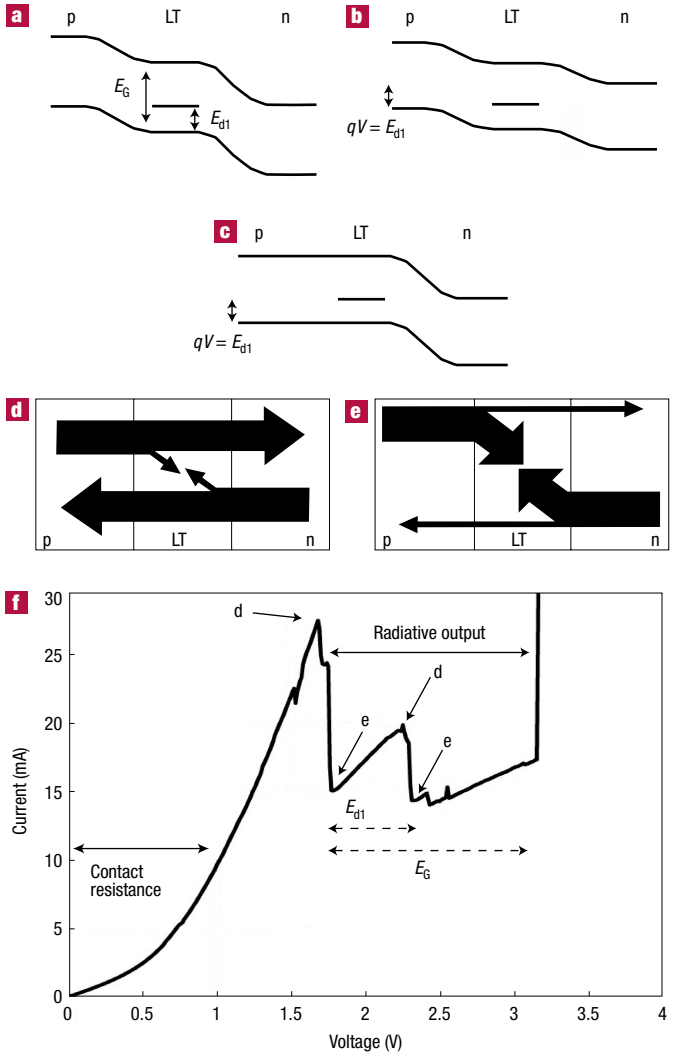

Figure 3 Energy bands, current flow, and measured current–voltage characteristic for our GaAs sample. a, Energy bands in equilibrium. **b**, Energy bands when the applied voltage is E_{d1}/q, and the voltage drop across the p–LT junction is about the same as that across the n–LT junction. **c**, Energy bands when the applied voltage is E_{d1}/q, and the voltage drops mainly across the p–LT junction. **d**, Current flow through the sample when there is little recombination in the LT layer. Most of the injected carriers reach the opposite contact. **e**, Current flow through the sample when there is much recombination in the LT layer. Most of the injected carriers do not reach the opposite contact. **f**, Measured current–voltage characteristic for the LTG-GaAs at room temperature. Parts c and b are associated, respectively, with the current peak and current valley at 2.25 V in part f.

terms of the symmetry, atomic-orbital admixture, and characteristic size of the deep state. The symmetry of the bound states of a spherically symmetric deep centre is found by writing the deep states as eigenstates of total angular momentum (spin plus Bloch plus envelope angular momenta). The conduction- and valence-band components of a deep state depend on the angular momentum quantum numbers, as well as the energy of the deep level relative to the conduction- and valence-band edges. Thus, the character of a mid-gap state is roughly half conduction -band-like and half valence-band-like. A precise calculation[3,4] of the oscillator strength indeed shows strong optical transitions from mid-gap states to both the conduction and valence band. This implies large device efficiency-bandwidth products. Quite generally, energy-band theory shows the deep-state radius to be about twice the Kane dipole[3,4]. In GaAs, this deep-state radius is approximately 1.3 nm. Thus, the deep-state radius is smaller than the Bohr radius of shallow impurities, but bigger than the nearest-neighbour distance. These general properties of symmetry, atomic orbital admixture, and radius of deep-states have been verified[3,4,8–10] by scanning tunnelling microscopy, and measurements of the selection rules, strength and spectral shape of deep-level optical transitions.

For devices, the current through the deep-level energy band would be larger when the deep-centre spacing is designed to be less than the diameter of the deep state. Larger deep-state radii are possible[3,4] for smaller bandgap materials, larger Kane dipole, and more shallow deep levels.

Device fabrication and measurement are described in the Methods section. This device was designed to efficiently inject holes into the valence band, and electrons into As_{Ga}^+ (E_{d1} in Fig. 2b[11]). Figure 3 shows the device energy bands in equilibrium and forward bias, as well as current paths. Figure 3f shows the current through the sample as a function of voltage. For voltages less than 1 V, the current–voltage characteristic is dominated by the Schottky-like n-contact. At 1.75 V, the current drops sharply, and optical emission is observed. Another 0.5 V higher, at 2.25 V, the current drops sharply again. This 0.5 V corresponds to the As_{Ga}^+ deep-level E_{d1} (0.5 eV above the valence band). At 3.15 V, the current rises sharply, and this 1.4 V difference from 1.75 V corresponds to the bandgap E_G (1.42 eV) of GaAs.

The sharp drop in the total current in Fig. 3f, and the accompanying optical emission, can be explained with the help of Fig. 3b–e. At those values of the voltage (1.75 V and 2.25 V) where the current drops sharply in Fig. 3f, the energy bands switch between two different line-ups, such as from Fig. 3b to Fig. 3c. Although the total voltage between the p- and n-layers is the same E_{d1}/q (where q is charge) in both Fig. 3b and c, the carrier recombination in the LT-layer is much higher in the case of Fig. 3c, where most of the voltage drops across the p–LT junction. The reason is that for the energy bands of Fig. 3c, electrons are efficiently injected from the n-layer into E_{d1} of the LT-layer, and holes are efficiently injected from the p-layer into the

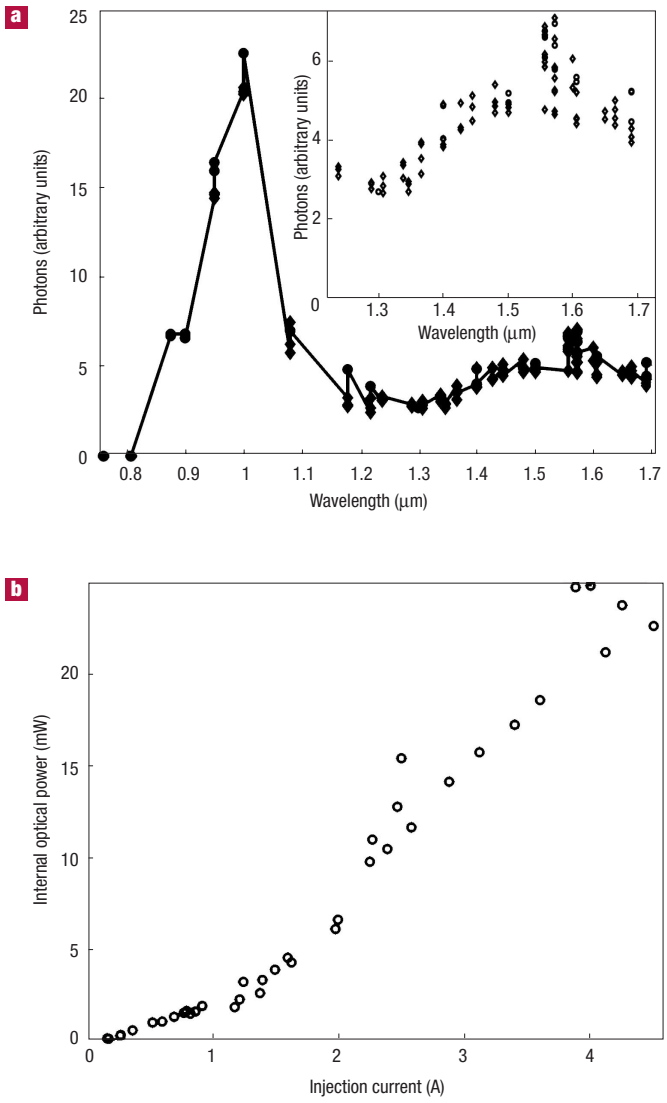

Figure 4 Room-temperature electroluminescence. a, Measured electroluminescence spectrum of LTG-GaAs at room temperature. The inset shows the measured electroluminescence between 1.2 μm and 1.7 μm. Both the absorption and the electroluminescence show transitions at 1.0 μm and 1.5 μm. **b**, Room-temperature electroluminescence measure d as a function of injection current.

valence band of the LT-layer. Figure 3e shows that when the recombination in the LT-layer is very large, the injected carriers do not reach the opposite contact and the total current through the device is much smaller than it would be if the recombination in the LT-layer had been small, as in Fig. 3d. Moreover, when the recombination in the LT-layer is increased, some of this recombination is radiative. Thus, it makes sense that when the recombination in the LT-layer increases sharply, the total current through the device drops sharply (points labelled 'e' in Fig. 3f) and optical emission is observed.

Figure 4a shows the first measurement of room-temperature electroluminescence from As_{Ga}. Figures 1 and 4a show that both the absorption and electroluminescence of LTG-GaAs indicate transitions at 1.0 μm and 1.55 μm, which correspond, respectively, to the transition between the conduction band and As_{Ga}^{+} and to the transition between As_{Ga} and the valence band in Fig. 2b. Conduction-band-to-As_{Ga}^{+} transitions increase the population of As_{Ga}, and As_{Ga}-to-valence-band transitions increase the population of As_{Ga}^{+}.

The measured optical signal radiated by our LED into the solid angle subtended by an *f*/1.5 lens was 32 μW for an injection current of 4.25 A. It follows that the optical signal radiated into 2π steradians of free space was 560 μW. This represents only 2.4% of the internal optical power within the sample, because the critical angle for total internal reflection is 17° for GaAs surrounded by free space[5]. This 2.4% is 1/4π times the solid angle subtended by a 17° angle of incidence, which implies that the internal optical power within the GaAs sample was 24 mW—a significant electroluminescent power. For comparison, the first quantum cascade laser[12] emitted 4 μW just below threshold, and 8.5 mW above threshold.

Figure 4b shows the measured electroluminescence as a function of injection current at room temperature. Significantly, the linear shape in Fig. 4b of the electroluminescence as a function of injection current is appropriate for a spontaneous emission process. For injection currents greater than 1 A, Fig. 4b indicates a measured efficiency of 6×10^{-3} photons per electron, which is 20 times the internal efficiency (3×10^{-4}) of the first quantum cascade laser[12] below threshold, and 60 times the internal efficiency (10^{-4}) of the first quantum cascade LED[13]. Assuming a radiative $\tau_R = 1$ ns, our internal efficiency implies a non-radiative $\tau_{NR} = 6$ ps. (The internal efficiency is, at most, $\tau_{NR}/(\tau_R + \tau_{NR})$.) At a lower injection current of 150 mA, we measured an internal efficiency of 2×10^{-4}. Thus, at this lower injection of 150 mA, the measured internal efficiency implies a non-radiative $\tau_{NR} = 200$ fs, which is consistent with an estimate of $\tau_{NR} = 500$ fs based on previous work[1,2] on the capture of holes by As_{Ga}. (Fig. 24 of ref. 2 shows the values of τ_{C1} and τ_{NR} in our Fig. 2b to be 10 ps and 50 ps for LTG-GaAs with 0.02% excess As. Because our LTG-GaAs has about 2% excess As, τ_{C1} and τ_{NR} are 100 fs and 500 fs, respectively.)

Both the turn-off time and the turn-on time (for example, decay[5–7] time of relaxation oscillations) of optical emitters are determined by the below-threshold total relaxation rate ($1/\tau_R + 1/\tau_{NR}$) of carriers from the upper state to the lower state of the optical transition. Our fast $\tau_{NR} = 200$ fs in the total relaxation rate ($1/\tau_R + 1/\tau_{NR}$) could make possible direct modulation of semiconductor lasers at terahertz speeds, something very desirable.

METHODS

DEVICE FABRICATION

The sample was grown in a molecular beam epitaxy system (EPI GENII, Veeco, Saint Paul, Minnesota, USA) on an n-type GaAs substrate. A GaAs buffer layer of 1 μm was grown at a substrate pyrometer temperature of 550 °C at 1 μm h^{-1} with a Si doping of 10^{19} cm^{-3} and a As_2-to-Ga beam equivalent flux ratio of 15. The substrate temperature was then lowered to 225 °C during the growth of 300 nm of GaAs at 0.5 μm h^{-1} and a Si doping of 3.5×10^{18} cm^{-3}. Then 400 nm of LTG-GaAs was formed at 225 °C at 0.5 μm h^{-1} with Si doping of 3×10^{18} cm^{-3}. Subsequently, the substrate temperature was raised to 350 °C during the first 100 nm of a 300 nm layer of undoped GaAs. The top layer was 200 nm of GaAs having a Be doping of 10^{20} cm^{-3} grown at a substrate temperature of 350 °C.

Standard photolithographic techniques were used to etch mesas, and to deposit titanium–gold contacts. The contacts were not annealed. The p-contacts were ohmic with a resistance between 2 Ω and 15 Ω. The n-contacts were weak Schottky diodes, which required about 0.5–0.8 V to reach milliampere currents.

ELECTROLUMINESCENCE MEASUREMENTS

Electroluminescence was measured in forward bias with 200 ns pulses and a duty cycle less than 10^{-4}. Two *f*/1.5 lenses were used with either a Newport 818IG InGaAs detector (Newport, Irvine, California) an InGaAs detector with transimpedance amplifier to calibrate the optical emission. Spectral measurements made with a JY Spex 1681B spectrometer (Jobin Yvon, Edison, New Jersey) were in agreement with those made with a set of narrow-bandwidth wavelength filters. The response of the detector, lenses and spectrometer (or wavelength filters) were divided out of the raw optical signal to obtain Fig. 4.

A control sample showed no electroluminescence. The control sample had the same growth sequence as the test sample, but had a growth interruption of 10 minutes at 225 °C just before the LTG-GaAs layer. This growth interruption produces, on the substrate side of the LTG-GaAs layer, an As-layer, which efficiently traps carriers.

Received 4 February 2003; accepted 28 March 2003; published 4 May 2003.

References

1. Melloch, M. R. *et al.* Low-temperature grown III-V materials. *Ann. Rev. Mater. Sci.* **25,** 547–600 (1995).
2. Melloch, M. R. *et al.* Molecular beam epitaxy of nonstoichiometric semiconductors and multiphase material systems. *Crit. Rev. Solid State Mater. Sci.* **21,** 189–263 (1996).
3. Pan, J. L. Optical emission from bound states of semiconductor deep-centres. *Opt. Express* **9,** 796–805 (2001).
4. Pan, J. L. Analytical method for finding the general optical properties of semiconductor deep centres. *J. Appl. Phys.* **92,** 5991–6004 (2002).
5. Agrawal, G. P. & Dutta, N. K. *Long Wavelength Semiconductor Lasers* 225, 244–247 (Van Nostrand Reinhold, New York, 1986).
6. Siegman, A. E. *Lasers* 119, 958, 962–964 (University Science Books, Mill Valley, California, 1986).
7. Marcuse, D. & Lee, T. P. On approximate analytical solutions of rate equations for studying transient spectra of injection lasers. *IEEE J. Quantum Electr.* **19,** 1397–1406 (1983).
8. Feenstra, R. M. Cross-sectional scanning tunneling microscopy of III-V semiconductor structures. *Semicond. Sci. Techol.* **9,** 2157–2168 (1994).
9. Feenstra, R. M., Woodall, J. M. & Pettit, G. D. Observation of bulk defects by scanning tunneling microscopy and spectroscopy: Arsenic antisites defects in GaAs. *Phys. Rev. Lett.* **71,** 1176–1179 (1993).
10. Grandidier, B. *et al.* Scanning tunneling microscopy and spectroscopy of arsenic antisites in low-temperature grown InGaAs. *Appl. Phys. Lett.* **74,** 1439–41 (1999).
11. Baraff, G. A. & Schluter, M. A. Electronic aspects of the optical-absorption spectrum of the EL2 defect in GaAs. *Phys. Rev. B* **45,** 8300–8309 (1992).
12. Faist, J. *et al.* Quantum cascade laser. *Science* **264,** 553–556 (1994).
13. Faist, J. *et al.* Mid-infrared field-tunable intersubband electroluminescence at room temperature by photon-assisted tunneling in coupled-quantum wells. *Appl. Phys. Lett.* **64,** 1144–1146 (1994).

Acknowledgements

We thank R. D. Grober for the use of his FTIR equipment for absorption measurements. J.L.P. was supported by National Science Foundation CAREER.

Correspondence and requests for materials should be sent to J.L.P.

Competing financial interests

The authors declare that they have no competing financial interests.